PHYSICAL SCIENCES

PRE-BREAKDOWN CURRENTS IN DIELECTRIC MATERIALS DURING ANODE ELECTRIC BREAKDOWN

Kulikov V.
Doctor of Phys.- Math. Sciences. Professor
Tomsk Agricultural Institute, Tomsk, Russia
https://doi.org/10.5281/zenodo.19573255

Abstract
The structure of pre-breakdown current in samples of crystalline NaCl, glass, polyethylene, water and transformer oil is considered. The primary breakdown current is caused by the mechanism of free electron generation through interatomic cascade Auger transitions in the valence band of the dielectric. The secondary current is associated with the movement of ions in the gas phase of the channel. The mechanisms of formation of primary and secondary breakdown currents are common in solid and liquid dielectric materials.

Keywords: pre-breakdown current, electrical breakdown, breakdown mechanism

Introduction

Electrical breakdown is characterized by a loss of electrical strength and the destruction of the dielectric. Research into the electrical breakdown process in insulating materials helps improve the power and reliability of high-voltage pulse power plants.

High breakdown channel velocities (10^5-10^8 cm/s) and low channel diameters (1-10 μm) create significant difficulties in the experimental study of the breakdown process. Direct studies of breakdown parameters include measurements of the conduction current [1-5], the velocity of movement of the breakdown channel front [1-9] and the mass composition of the gas phase [10, 11]. In experiments, recording pre-breakdown currents at the voltage pulse front is associated with the need to use bridge measurement circuits to compensate for capacitive recharge currents [1, 2, 4]. Alternatively, the pre-breakdown current structure can be distinguished against the background of the discharge curve of the electrical circuit.

Electrical breakdown from the anode (anodic breakdown) in solid [12-22] and liquid dielectrics [23-26] is satisfactorily described by the mechanism of cascade Auger transitions in the valence band of the dielectric. The appearance, movement, and orientation of the electrical breakdown channel are determined taking into account data on the crystal-chemical and energy structure of the substance.

The application of the concept of the band structure of a substance implies the presence of short-range and long-range order in the crystal lattice of a sample. Long-range order ensures the band nature of carrier motion in a crystal, in contrast to the hopping nature in amorphous substances. Short-range order plays a major role in determining the energy spectrum of a material [27]. The quasi-crystalline structure of solid and liquid organic dielectrics arises from the ordering of long molecules, when the molecules are located more or less parallel to each other [28]. In this case, the energy levels of the highest occupied molecular orbital (HOMO) correspond to the upper edge of the valence band W_v, and the lowest unoccupied molecular orbital (LUMO) correspond to the lower edge of the conduction band W_c. The highest occupied molecular orbital HOMO and the lowest unoccupied LUMO are separated by a band gap [28].

According to [12-16], the conduction current is caused by the mechanism of free electron generation via interatomic Auger transitions in the valence band of the dielectric. Carrier recombination results in heating and the formation of a gas phase in the breakdown channel. Secondary processes are associated with the destruction of the channel surface by bombardment with accelerated ions in a strong non-uniform field and the impact multiplication of ions during collisions with conglomerates of atoms of the substance in the region of its gas phase. The movement of ions creates a secondary breakdown current. The electrical parameters of the currents in samples of single-crystal NaCl and liquid water are presented in [22, 25, 26].

In this paper, the processes of formation of primary and secondary currents of anodic electrical breakdown are considered in a wider range of dielectric materials.

Model of electrical breakdown in crystalline NaCl

Generation of free charge carriers

The diagram of energy bands in the contact region of a metal electrode and a NaCl sample in a strong electric field is shown in Fig. 1. The crystal is oriented in the <110> direction. The energy levels of the states of Na and Cl atoms are given in accordance with the data of [29].

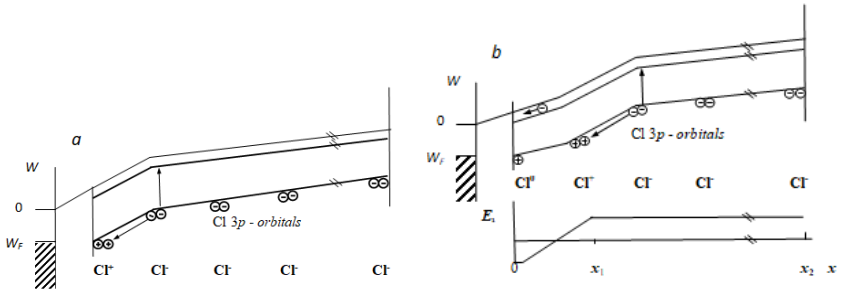

Fig. 1. Schematic of Auger transitions in NaCl in a strong electric field. W_F - energy levels of the Fermi metal; E_1 - space charge electric field

According to [15-16], the onset of breakdown channel formation is determined by processes at the metal-dielectric interface. With an average field strength in the sample of ~ 10^6 V/cm, the actual field strength near the electrode microtips can be greater than ~10^8 V/cm. In the near-electrode region of the dielectric, Cl^+ ions with two holes in the 3p orbitals are formed due to the tunneling transition of electrons into the metal. This requires a voltage *U* such that the edge of the valence band of the dielectric rises to the Fermi level of the metal. In a NaCl crystal, an electron at the 2p level of Na^+ is located ~ 22.4 eV below the bottom of the band gap and does not participate in the recombination of a hole into Cl^+. The decay of a hole into Cl^+ occurs as a result of the interatomic Auger transition of an electron from the 3p orbital of an adjacent Cl^- atom and the subsequent generation of an Auger electron into the conduction band (Fig. 1,a). The Auger transition is possible under the condition that the minimum energy gap between the 3p levels of chlorine in an electric field is not less than the band gap of the dielectric *W*g=8.8 eV. The necessary band bending for the Auger transition at a distance close to the interatomic distance is provided by the local electric field of the space charge (SC) and, first of all, the layer of doubly positively charged ions of the halide Cl^+ [16, 20].

A single cycle of the discharge front movement in a NaCl crystal can be divided into two successive stages. In the first stage, when the critical local electric field strength of ~10^8 V/cm is reached, hole recombination on Cl^+ occurs due to the interatomic Auger transition of an electron from an adjacent chlorine atom over a time of τ_A ~10^{-16} s and the generation of an Auger electron into the conduction band of the dielectric. The channel advances by one interatomic distance (Fig. 1,a). The negative charge of the electrons reduces the hole charge field and, accordingly, the band bending near the conduction band boundary. The second stage is associated with the extraction of electrons from the discharg region by the external electric field and the achievement of the critical field strength for the next cycle. Cycle time Δt can be represented

$$\Delta t = \tau_A + \tau_1, \quad (1)$$

where τ_1 is the time to reach the critical electric field strength.

In NaCl crystals, Auger transitions propagate along the Cl^- - Cl^- ion chain (Fig. 1,b). The spatial structure of the breakdown channel is formed by a set of individual Auger transition channels (Fig. 1) extending in the same direction. This mechanism ensures high stability of the breakdown channel's transverse dimensions in alkali halide crystals over a fairly long length (Fig. 2).

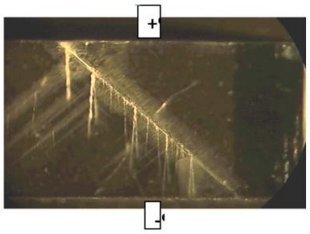

Fig. 2. Channel of pulsed anodic breakdown in crystalline NaCl. Electrode configuration: positive needle – plane [14]

It should be noted that long chains of Cl^- - Cl^- ions (passing through the entire crystal) ensure stable movement of the breakdown channel without breaks (Fig. 2).

The channel comprises a positive space charge, a heated layer of material, and a conductive region of complex phase composition with electron-hole plasma. The channel front moves from the positive electrode into the sample.

The channel diameter is probably determined by the size of the layer of Cl^+ ions in the near-surface area of the dielectric, and is proportional to the external voltage. According to [7], the breakdown channel diameter in KCl and KBr samples increases linearly with the voltage in the range of 100-300 kV. The breakdown channel movement may be delayed by the formation of the surface layer of Cl^+ ions.

Formation of space charge

The formation of a space charge at the boundary of the conducting layer 0 - x_1 (Fig. 1,*b*) and an electric

current in a metal-insulator-metal structure are considered. The continuity equation (2) and Poisson's equation (3) were used in the calculation.

$$\frac{\partial \rho}{\partial t} = G - \frac{\partial}{\partial x}\left(en\mu E\right), \quad (2)$$

$$\frac{\partial E}{\partial x} = \frac{\rho}{\varepsilon\varepsilon_0}, \quad (3)$$

where n and p are concentrations of free electrons and immobile holes; e and μ are the electric charge and electron mobility, $\rho = e(p - n)$ is the space charge density; $E = E_0 + E_1$ is the total electric field strength ($E_0=U/x_2$ and E_1 are the values of the strength of the external electric field and space charge, respectively); ε and ε_0 are the values of the dielectric permittivity of the sample and electric constant, respectively; $G = en_1/\tau_A$ is the volume rate of the Auger electron charge generation in the space from x_1 to $x_1 + \Delta x$ (n_1- initial concentration of Auger electrons, Δx is the atomic layer thickness in the crystal ~ 4 Å). t_0 is the time of switching on the generation of Auger electrons at the moment of reaching the critical field strength.

The initial and boundary conditions of the problem will be as follows:

at $t = 0$, the field strength $E = 0$, (4)

at $x \geq x_1$, $\sigma = 0$, denote $E_1 = E_s(t)$, (5)

where $E_s(t)$ is the electric field strength beyond the space charge boundary x_1, $\sigma = en\mu$ is the conductivity. After the transformations (2) and (3), we get

$$\varepsilon\varepsilon_0 \frac{\partial^2 E}{\partial x \partial t} = G - \sigma \frac{\partial E}{\partial x}. \quad (6)$$

The integration (6) on the x coordinate using the boundary condition (5) gives

$$\varepsilon\varepsilon_0 \frac{\partial E}{\partial t} = G\Delta x - \sigma E_0 - \sigma E_1 + \varepsilon\varepsilon_0 \frac{\partial E_s}{\partial t}. \quad (7)$$

The short-circuiting condition takes the form (8)

$$\int_0^{x_2} E_1 dx = 0. \quad (8)$$

To a first approximation, the equation (8) can be written as

$$E_1 x_1 + E_s(x_2 - x_1) = 0. \quad (9)$$

To find E_1 in (7), we shall express E_s in terms of E_1 and integrate the equation (7) with respect to x from x=0 to x_2.

$$\varepsilon\varepsilon_0 \int_0^{x_2} \frac{\partial E_1}{\partial t} dx = \int_{x_1}^{x_1+\Delta x} G\Delta x dx - \sigma \int_0^{x_1} E_0 dx - \sigma \int_0^{x_1} E_1 dx - \varepsilon\varepsilon_0 \frac{x_1}{\left(x_2 - x_1\right)} \int_0^{x_1} \frac{\partial E_1}{\partial t} dx. \quad (10)$$

Given the short-circuiting condition (8), we obtain

$$\frac{\partial E_1}{\partial t} + \frac{E_1}{\tau} = -\frac{E_0}{\tau} + \frac{G\Delta x^2}{\sigma x_1 \tau}, \quad (11)$$

where $\tau = \tau_m x_1/(x_2-x_1)$ is the circuit time constant, $\tau_M = \varepsilon\varepsilon_0/\sigma$ - Maxwell relaxation time. The solution to the equation (11) for E_1 is found to be

$$E_1 = -E_0\left(1 - exp\left(-\frac{t}{\tau}\right)\right) + \frac{G\Delta x^2}{x_1\sigma}\left(1 - exp\left(-\frac{\tau_A}{\tau}\right)\right). \quad (12)$$

A decrease in the field strength of the positive space charge E_1 occurs as a result of the actuation of the Auger electron field. Without the Auger generation, the field strength E in the sample region 0 - x_1 is given by

$$E = E_0\, exp\left(-\frac{t}{\tau}\right). \quad (13)$$

In the space x_1 - x_2, the field strength of the space charge E_s with regard to (9) is written as

$$E_s = \frac{E_0 x_1}{\left(x_2 - x_1\right)}\left(1 - exp\left(-\frac{t}{\tau}\right)\right). \quad (14)$$

The field strength E_s increases superlinearly with increasing coordinate x_1.

. The value of the positive space charge Q_s is determined as

$$\varepsilon\varepsilon_0 E_s = Q_s\left[\frac{k}{cm^2}\right]. \quad (15)$$

The spatial structure of the electric field E_1 of charge Q_s in the 0-x_2 region is shown in Fig. 1.

Pre-breakdown conduction current

In a metal-insulator-metal structure, when voltage is applied, the conduction current density in the 0-x_1 space is

$$i_1 = \sigma E = \sigma E_0 \exp(-t/\tau). \quad (16)$$

The displacement current density in the space x_1 - x_2 has the form

$$i_s = \frac{\partial Q_s}{\partial t} = \sigma E_0\, exp\left(-\frac{t}{\tau}\right). \quad (17)$$

Conduction current (16) and bias current (17) are equal. Currents (16) and (17) arise when space charge Q_s forms at boundary x_1 ($\sigma = 0$). Equation (16) reflects the fact that, at the moment the voltage is applied, current i_1 is equal to σE_0 and decreases exponentially with time.

The generation of Auger electrons creates a conductive layer in the region $x_1 + \Delta x$. An electric current subsequently arises when space charge forms at the boundary $x_1 + \Delta x$ under the influence of an external field E_0. In equation (16), the relaxation time t is limited by the onset of the next Auger transition after time τ_1 at time $t = t_0$. In the breakdown channel motion model, equation (16) can also be viewed as the dependence of the current density on the position of space charge $Q_s(x_1)$ in the sample at a time other than $t = 0$. The dependence of the conduction current density function (16) on the argument x_1 in coordinates $t_1 = x_1/v$ (where v is the breakdown channel velocity and $t_b = x_2/v$ is the breakdown time) for fixed times $t_{01} = 0.1\ \tau_M$ (curve 1), $t_{02} = 0.05\ \tau_M$ (curve 2), and $t_{03} = 0.01\ \tau_M$ (curve 3) is shown in Figure 3.

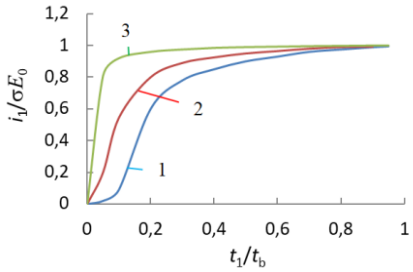

Fig.3. Dependence of the conduction current density function in the breakdown channel on the channel travel time

The current amplitude (curves 1-3) increases with decreasing argument t_0, which occurs with increasing channel velocity. The current density (curve 3) increases slightly with increasing coordinate x_1.

Breakdown channel movement speed

The time taken to reach the critical field strength τ_1 in the equation (1) can be found from the relationship

$$\tau_1 = Q_A/i_1 \text{ , (18)}$$

where Q_A - is the charge density of Auger electrons according to the equation (12)

$$Q_A = \varepsilon\varepsilon_0 \frac{G\Delta x^2}{x_1\sigma}\left(1-exp\left(-\frac{\tau_A}{\tau}\right)\right). \text{ (19)}$$

Carrier injection occurs in a short time and does not depend on the field strength E_0.

$$\Delta t = \tau_A + \frac{G\Delta x^2\tau_m}{E_0 x_1\sigma}\exp\left(\frac{t_0}{\tau}\right)\left(1-\exp(-\frac{\tau_A}{\tau})\right). \text{ (20)}$$

The formula for Δt makes it possible to estimate the dependence of the channel velocity $v(x_1) \approx \Delta x/\Delta t$ on the field strength E_0, conductivity σ, and coordinate x_1.

Electrical breakdown parameters

The oscillograms of voltage U and pre-breakdown current I in a NaCl crystal with a thickness of d = 2 mm and a positive polarity of the needle electrode are shown in Fig. 4 [1]. A bridge circuit was used to compensate for capacitive currents. In the needle -plane structure of the electrodes, the distribution of E_x is non-uniform and decreases hyperbolically across the sample [1]. The average electric field strength $E_{mid} = U/d$ [30].

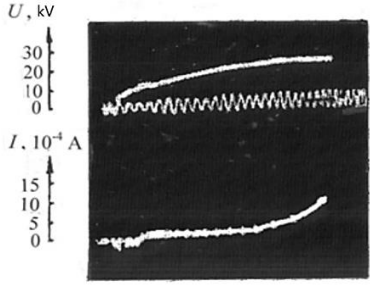

Fig. 4. Oscillograms of the voltage pulse U and current I in a NaCl crystal [1]

The onset of discharge propagation is indicated on the oscillograms by the appearance of a current of approximately ~$2\cdot10^{-4}$ A (Fig. 4) [1]. As the discharge advances deeper into the sample, the current amplitude remains constant and, after 1/2 the breakdown time, increases exponentially. The maximum current of ~10^{-3} A corresponds to the time the breakdown channel reaches the cathode. This is followed by a sharp increase in current, which is not reflected in the photograph. According to [1], the breakdown channel diameter expands near the anode to ~2-3 μm and narrows towards the cathode to ~0.5-1 μm.

As shown above, the pre-breakdown current amplitude can increase by no more than a few percent as the channel passes through the sample. The primary current density is $i \approx 2\cdot10^4$ A/cm^2 for a channel diameter of 1 μm. At an average field strength E_{mid} ~10^5 V/cm, the breakdown front velocity $v \approx 10^6$ cm/s, conductivity $\sigma = i/E_{mid} \approx 0.2$ Ohm^{-1} cm^{-1}.

According to [1], electrical breakdown in NaCl, KCl, KBr crystals of different thicknesses at the selected value of E_{mid} ~10^5 V/cm is characterized by a stable amplitude of the primary current ~$2.8\cdot10^{-4}$ A. With an increase in the length of the sample, the breakdown time and the amplitude of the maximum current increase.

Secondary breakdown effects

An increase in the channel diameter near the anode surface of the NaCl sample was noted in [1].

The destruction of the channel surface is probably associated with its bombardment by ions accelerated in a strong non-uniform field in the gas phase region of the discharge. In general, ion sputtering begins when the ion energy W_i exceeds the threshold value W_b. The value of W_b weakly depends on the mass of the colliding particles and is in the range of ~10-30 eV [31]. The efficiency of the sputtering process increases with the increase in the mass of the bombarding ions, the angle of incidence of ions from 0 to 40-70^0 and the energy W_i to 70-80 eV [31]. A model of sputtering of two-component materials by light ions is presented in [32]. According to the model, the outgoing flow of atoms is associated with the movement of a certain conglomerate of atoms of both components.

Mass spectrometry studies of plasma clots ejected into a vacuum from the surface overlap region and from breakdown channels in solid dielectrics show that the bulk of the ionic charge is carried by singly ionized

molecules. In the case of KCl, these are KCl^+, K_2Cl^+, and $(K_2Cl_2)^+$ ions [10]. The degree of ionization in the breakdown channel in such cases does not exceed 10%. It can be assumed that the bulk of neutral particles have the same composition [10].

In NaCl samples, the impact particles are most likely Na^+ ions, and the sputtered particles are $NaCl^+$ conglomerates. Specifically, for positive ions, there is an angular component of the field strength relative to the channel wall surface. The gas phase includes neutral and positively charged ions and conglomerates of the original substance's atoms.

The increase in channel diameter and current buildup in the experiment (Fig. 4) can be attributed to secondary breakdown effects. The nature of the current increase corresponds to the exponential law $I(t)\sim 2^n$ (where n is an integer). The onset of the current is shifted by a time t_g and is likely associated with the onset of gas phase formation. The drift velocity v_d of a charged particle in the gas phase in a nonuniform electric field E_x is determined as

$$v_d = \mu E_x . \quad (22)$$

The superlinear rise in the current *I(t)* in Fig. 4 is satisfactorily described by the sum of stair step functions:

$$I(t) = \sum_i^M I_i \left(t_g + \Delta t_i \right) , \quad (23)$$

where *i*- number of a claster of charged particles; I_i – current with initial carrier concentration N_0; M — total amount of currents I_i; t_g – time to the creation of gas phase, Δt_i – time lag between the start of the current flow and t_g. We have designated the number of steps as k and the duration of the step as t_k. The equation (23) is satisfied if the time lags Δt_i lie in the narrow time margin $\Delta t_i < t_k$.

The function of current I_1 created by the bunch of the charged particles in sample NaCl is presented in Fig.5.

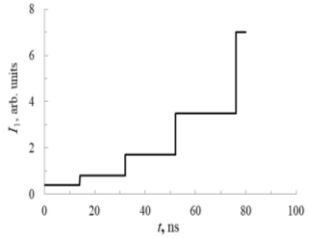

Fig. 5. View of the current function I_1 during impact multiplication of charged particles in a NaCl sample

A characteristic feature of the current structure is its periodic doubling at each time interval $i_{\square}$, which corresponds to the process of impact disintegration of conglomerates of atoms of the substance during bombardment with fast particles. The increase in the duration of the charged particle acceleration period $t_{\square\square}$ correlates satisfactorily with a decrease in the amplitude of the electric field strength E_x in the tip-plane electrode system. This indicates the movement of an avalanche of positive ions from the anode electrode into the sample.

Sufficiently large values of $t_{\square}$ probably include the times of the process of spraying the channel walls with the formation of $NaCl^+$ conglomerates and the subsequent reaction of impact multiplication of Na^+ ions according to the scheme

$$Na^+ \rightarrow NaCl = Na^+ + NaCl^+, Na^+ \rightarrow NaCl^+ = 2Na^+ + Cl^0 . \quad (24)$$

The rate of reaction (24) is likely limited by the time it takes for conglomerates to form.

For a sodium chloride sample, the number of acceleration cycles at half the channel length is $k = 4$, and the gas phase formation time is $t_g \approx 80$ ns. The average path between two shock generation events, z_{mid}, is ~0.25 mm. The last acceleration cycles (Fig. 5) are close in time and correspond to motion in the mean field region E_{mid}. The drift velocity in this region for sodium ions is $v_d \approx z_{mid}/ t_{\square} \sim 1.2\cdot 10^6$ cm/s.

The kinetic energy of the ions Na^+ in the region of the average electrical field strength is ~10 eV. The amount of energy is probably enough to sustain impact multiplication of ions during the destruction of aggregates in the gas phase. Mobility of Na^+ ions in the gas phase of the breakdown channel in the region of average electrical field strength is equal to $\mu \approx 12$ cm^2/Vs, according to formula (22).

The current density in the region of average field strength (k=3) is $i_3 \approx 1.7\cdot 10^4$ A/cm^2 (Fig. 4), the carrier multiplication factor is *B=4*. The current density can be represented as $i_3 = eN_3v_d$, which gives the ion concentration $N_3 \approx 8\cdot 10^{16}$ cm^{-3}. Considering that *B=4*, the sodium ion concentration near the anode is $N_1 \approx 2\cdot 10^{16}$ cm^{-3}. In formula (23), the initial ion concentration N_0 can be taken to be equal to $0.1\cdot N_1$, while the number of currents M is equal to 10.

Pre-breakdown currents in glass

A study of the pre-breakdown current in a glass sample is presented in [1]. Measurements were performed using voltage pulses with a rise time of 0.2-3 μs, in a non-uniform field, and with a positive tip polarity. A bridge circuit was used to compensate for capacitive currents. Oscillograms of voltage U and pre-breakdown current I in a glass sample ~5 mm thick are shown in Fig. 6 [1].

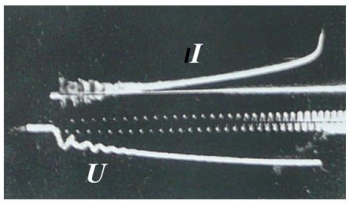

Fig.6. Oscillogram of the voltage pulse U and current I in a glass sample [1]

When the voltage reaches the breakdown value, a current of ~$1.6 \cdot 10^{-4}$ A is observed on the oscillogram [1]. As the discharge progresses deeper into the sample, the current amplitude remains constant and, after 0.3 of the breakdown duration, increases exponentially to ~$20 \cdot 10^{-4}$ A.

Glass is an amorphous substance with preserved short-range order of the crystal lattice of the sample. The primary processes of the breakdown channel are associated with Auger transitions of electrons along the chain of nearby oxygen ions and the generation of electrons in the conduction band, as occurs in a quartz crystal [17]. The superlinear increase in current is related to secondary phenomena in the gas phase of the discharge. The accelerated particles are likely silicon ions.

Pre-breakdown currents in polyethylene

The electronic properties of organic dielectrics are conditioned by the presence of covalent bonds with sp^3 - hybrid orbitals of the carbon atom [28]. In polyethylene, each atom of the carbon builds four σ - bonds with the neighboring atoms. The σ-bond is formed by overlapping sp^3 - hybridized orbitals, two with carbon atoms and the other two with hydrogen atoms. The energy spectrum of σ - electrons consists of levels that are filled with electrons and those that are not. The highest occupied molecular orbital HOMO and the lowest unoccupied molecular orbital LUMO are separated by a band gap. Opinion of the authors of [33], *W*g one can consider ~8 eV for polymer insulators

According to the works [15-16], during anode-initiated breakdown, the generation of free electrons and holes is caused by the Auger transition of electrons in the valence band of the dielectric. In polyethylene, the electron transfer occurs along the chain of C- C atoms oriented in the direction of the maximum electric field strength [20]. Some of the electrons recombine with holes with the release of heat. The released energy is spent on breaking chemical bonds and forming free macromolecules. Thermal pressure forms a hollow channel with the gas phase. Macromolecules disintegrate into ions under the action of thermal collisions [20]. Mass spectrometry of plasma clots ejected into a vacuum from the region of the surface breakdown channels in polyethylene shows that the main part of the ionic charge is carried by singly ionized clusters $C_2H_5^+$, $C_4H_9^+$, $C_8H_{17}^+$. The degree of ionization in the breakdown channel in such cases does not exceed 10% [11].

An experimental study of the pre-breakdown current in polyethylene samples with a needle-plane electrode configuration was conducted in [5]. A light-emitting diode connected to the sample's discharge circuit was used to record the current. The LED's glow intensity was proportional to the current. A bridge circuit for compensating capacitive recharge currents was not used.

According to [5], for samples with a thickness of ~1.49 mm, the pre-breakdown current appeared at the leading edge of a positive voltage pulse with an amplitude of ~60 kV. The voltage pulse duration was 760 ns. The average field strength in the sample, E_{mid}, was ≈$4 \cdot 10^5$ V/cm.

The breakdown tree is shown in Fig. 7. In this case, partial breakdown is observed. The maximum breakdown channel length is ~0.4 mm. The channel diameter is ~10 μm at the positive electrode and ~1 μm deep within the sample.

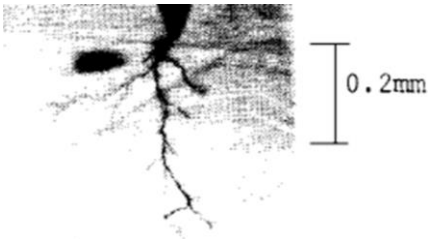

Fig. 7. The breakdown tree in polyethylene [5]

The current curve is highlighted against the background of the transient discharge current curve of the circuit. The pre-breakdown current trace is shown in Fig. 8.

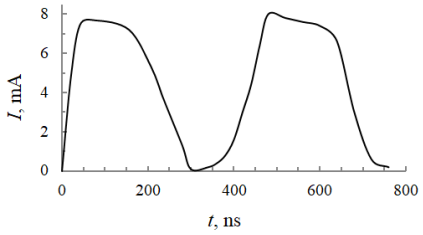

Fig. 8. The pre-breakdown current in polyethylene

The conduction current increased linearly from zero to ~7.6 mA over a period of ~50 ns. It then decreases to 7 mA at 170 ns and drops sharply to virtually zero at 300 ns. The first current pulse, 300 ns in duration (Fig. 8), corresponds to the primary breakdown current. With a channel diameter of ~10 μm (near the positive electrode), the current density is $\sim 7 \cdot 10^3$ A/cm^2, and the channel front velocity is $1.3 \cdot 10^5$ cm/s.

The increase in channel diameter and the increase in current $I(t)$ in the 300-480 ns range (Fig. 8) can be attributed to secondary breakdown effects. The superlinear increase in secondary current $I(t)$ in Fig. 8 is satisfactorily described by the sum of step functions in the form of equation (23). The form of the function I_1 is shown in Fig. 9.

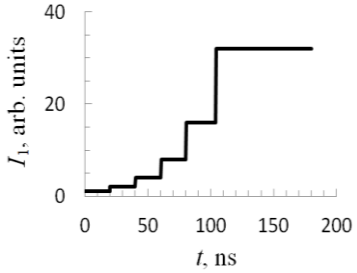

Fig. 9. View of the current function I_1 during impact multiplication of charged particles in polyethylene sample

A characteristic feature of the current structure is its periodic doubling at each time interval t_k, which corresponds to the process of impact disintegration of conglomerates of atoms of the substance when bombarded by fast particles.

Probably, in polyethylene, H^+ ions act as impactors, while $C_2H_5^+$ aggregates are sputtered. The process of sputtering the channel walls with the formation of $C_2H_5^+$ conglomerates and the subsequent reaction of impact multiplication of H^+ ions occurs according to the scheme

$$H^+ (- C_2H_2 - C_2H_2 -)_n = H^+ + C_2H_5^+, H^+ C_2H_5^+ = 2 H^+ + C_2H_4^0 . \quad (25)$$

The relatively large values of t_k are likely due to the formation of $C_2H_5^+$ conglomerates.

The number of acceleration cycles per channel length of 0.4 mm is $k = 5$ and the gas phase formation time is $t_g \approx 300$ ns. The average path between two shock generation events, z_{mid}, is ~0.08 mm. The last acceleration cycles (Fig. 9) are close in time and correspond to motion in the mean field region E_{mid}. The hydrogen ion drift velocity in this region is $v_d \approx z_{mid}/t_3 \approx 4 \cdot 10^6$ cm/s. Mobility of H^+ ions in the gas phase of the breakdown channel in the region of average electrical field strength is equal to $\mu \approx 10$ cm^2/V·s, according to formula (22).

Pre-breakdown currents in water

A model of the breakdown channel motion in a liquid water sample is presented in [24,26]. The basic idea of this approach is that, at close range, the structure of water is the same as that of hexagonal ice I_h. According to [24], during anodic-initiated breakdown, the generation of free electrons and holes is caused by the Auger transition of electrons in the valence band of the dielectric. In a water sample, electron transfer occurs along the O-H-O atomic chain, oriented in the direction of maximum electric field strength [24,26].

Figure 10 gives us some information on channel diameter and the velocity of its propagation in a water gap at $d = 0.8$ mm in a homogeneous field ~2 MV/cm, according to [34]. The time between the frames is ~1 ns, the average velocity of expansion of the glowing region is $\sim 10^7$ cm/s. The length and the diameter of the glow near the anode increase superlinearly in the channel's propagation process towards the cathode. The diameter of the channel near the anode at the initial stage of the breakdown is $d_k \approx 80$ μm (see Fig. 10).

Fig.10. Change in the length and diameter of the anode glow over time during breakdown in water [34].

The dependence of the current on time during breakdown in a 1 cm thick water layer is shown in Fig. 11 [4]. A bridge circuit was used to compensate for capacitive currents.

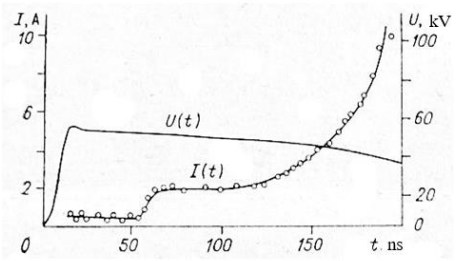

Fig. 11. Pre-breakdown current in water and voltage on the measuring capacitor [4]

The rise in current at ~50 ns corresponds to the beginning of the channel growth from the needle. At the initial stages of the expanding of the conduction area in the bulk of the sample the current remains stable (~2 A) until the length expands to ~5 mm, i. e. approximately a half of the distance from the tip of the needle electrode to the plane electrode. After that, the current increases by several times before the conducting channel spans the interelectrode gap. At the average electrical field strength of $\sim 5 \cdot 10^4$ V/cm, the breakdown channel front propagation velocity is $\sim 6.7 \cdot 10^6$ cm/s. The conductivity current density in water is $\sim 3 \cdot 10^4$ A/cm^2, conductivity $\sigma \approx 0.6$ Ohm^{-1} cm^{-1} at $d_k \approx 80$ μm.

The widening of the breakdown channel and the increase in current in the experiment (Fig. 11) can be attributed to secondary breakdown processes. The superlinear increase in current $I(t)$ in Fig. 11 is satisfactorily described by the sum of step functions in the form (23). The current function of a cluster of charged particles I_1 in a water sample is shown in Fig. 12.

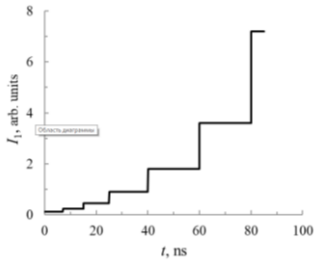

Fig. 12. Current function I_1 for impact multiplication of charged particles in a water sample

Most likely, in water samples, the impact particles are H^+ ions, and the H_2O^+ conglomerates are sprayed.

The rather large values of t□□□likely include the times of the process of spraying the channel walls with the formation of H_2O^+ conglomerates and the subsequent reaction of impact multiplication of H^+ ions according to the scheme

$$H^+ \rightarrow H_2O = H^+ + H_2O^+, H^+ \rightarrow H_2O^+ = 2H^+ + OH^0 \quad (26)$$

The reaction rate (26) is probably limited by the time of the formation of the aggregates.

The amount of the acceleration cycles at half of the channel length for water is k=6, and the time of gas phase formation is $t_g \approx 80$ ns. The average path between two acts of impact generation of ions z_{mid} in water is ~0.83 mm. The last cycles of acceleration (Fig. 12) are close in duration and correspond to the motion in the region of average field E_{mid}. The drift velocity in this region for water is $v_d \approx z_{mid}/t_4 \approx 5.5 \cdot 10^6$ cm/s. The kinetic energy of the ions H^+ in the region of the average electrical field strength is ~15.6 eV. The amount of energy is probably enough to sustain impact multiplication of ions during the destruction of aggregates in the gas phase. Mobility of H^+ ions in the gas phase of the breakdown channel in the region of average electrical field strength is equal to $\mu \approx 110$ cm^2/V·s, according to formula (22).

The current $I(t)$ in the region of average field strength (k=4) is ~0.9 A (Fig. 11). Current density is $i_4 \approx 1.1 \cdot 10^4$ A/cm^2 at the channel diameter d_k~0.1 mm and the carriers multiplication coefficient B=8. Current density may be presented in $i_4 = eN_4v_d$, where ion concentration $N_4 \approx 1.3 \cdot 10^{15}$ cm^{-3}. Considering that B=8, the concentration of hydrogen ions near the anode is equal to $N_1 \approx 1.6 \cdot 10^{14}$ cm^{-3}. In formula (23) the initial ion concentration N_0 may be assumed to be equal to $0.1 \cdot N_1$, whereas the number of currents M equals 10.

Pre-breakdown currents in transformer oil

Typical liquid dielectrics include alkanes, perfluoroeicosane, and others. The molecular model of naphthenic mineral oil [35] includes different types of alkanes: monocyclic $C_{14}H_{28}$ (32%), tricyclic $C_{16}H_{28}$ (26%), bicyclic $C_{13}H_{24}$ (18%), acyclic $C_{12}H_{26}$ (13%) and tetracyclic $C_{16}H_{26}$ (11%), which gives the density of 0.95 g/cm^3. Calculations of the electronic structure of mineral oil ab initio are presented in paper [28]. The valence and conduction bands of mineral oil are formed by the energy levels of the HOMO and LUMO states of alkane molecules, respectively. Forbidden band width is 6 eV [35].

The patterns of anodic breakdown in perfluoroeicosane are satisfactorily described by a mechanism based on cascade Auger transitions in the valence band of the dielectric [23].

A study of the pre-breakdown current in a transformer oil sample is presented in [2]. Measurements were performed by applying a pulsed voltage of 41.4 kV to a sample ~4 mm thick in a non-uniform field with a positive polarity of the needle tip. A bridge circuit was used to compensate for capacitive currents. The current

was recorded by a light-emitting diode included in the sample discharge circuit. The LED glow intensity is proportional to the current. An oscillogram of the pre-breakdown current *I* is shown in Fig. 13 [2].

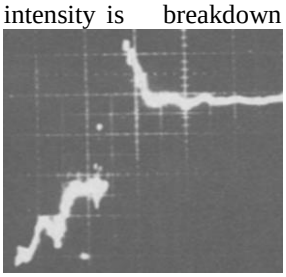

Fig. 13. Oscillograms of current pulse I in transformer oil. Current ~7 mA/div, time ~1 μs/div [2]

The primary conduction current increases with time to a maximum amplitude of 5.3 mA at 250 ns and decreases slightly as the breakdown channel moves. The secondary current appears 500 ns from the onset of the breakdown process and increases to 8.8 mA within 250 ns. A sharp increase in current at 1.4 μs then corresponds to the discharge current through the sample. In the experiment, the field strength E_{mid} was ~ 10^5 V/cm, and the breakdown channel velocity was $2.9 \cdot 10^5$ cm/s. The current density was $2 \cdot 10^4$ A/cm^2, the electron conductivity was 0.2 Ohm-1 cm^{-1} with a channel diameter of 5 μm. The secondary current is likely due to the movement of light hydrogen ions.

In paper [3], measurements of the pre-breakdown current in transformer oil were made under experimental conditions similar to those in [2]. A voltage of 43.3 kV was applied to a 5 mm thick dielectric layer with a positive needle-plane electrode configuration. The breakdown time was 2 μs. A light-emitting diode connected to the sample's discharge circuit was used to record the current. A bridge circuit for compensation of capacitive currents was not used. The pre-breakdown current trace is highlighted against the discharge curve (Fig. 14).

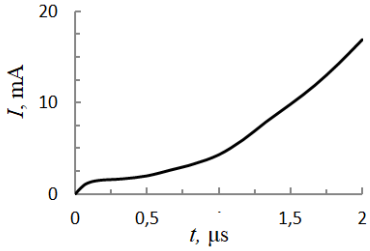

Fig. 14. The pre-breakdown current in a transformer oil sample

In the experiment, the average field strength in the sample was ~ $0.9 \cdot 10^5$ V/cm, the breakdown channel velocity was $2.5 \cdot 10^5$ cm/s. The primary current amplitude was ~ $1.5 \cdot 10^{-3}$ A. The current density was $0.6 \cdot 10^4$ A/cm^2, the electron conductivity was 0.07 Ohm^{-1} cm^{-1}, and the channel diameter was 5 μm.

A secondary current arises after 150 ns of breakdown. The current amplitude increases exponentially to ~$17 \cdot 10^{-3}$ A. The superlinear increase in current $I(t)$ in Fig. 14 is satisfactorily described by the sum of step functions in the form of equation (23). The current function of a cluster of charged particles I_1 in a transformer oil sample is shown in Fig. 15.

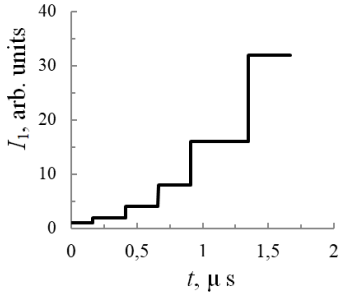

Fig. 15. Current function I_1 for impact multiplication of charged particles in a transformer oil sample

The impacting particles are likely hydrogen ions.

The amount of the acceleration cycles at half of the channel length for transformer oil is k=6, and the time of gas phase formation is $t_g \approx 150$ ns. The average path between two acts of impact generation of ions z_{mid} in transformer oil is ~0.83 mm. The last cycles of acceleration (Fig.15) are close in duration and correspond to the motion in the region of average field E_{mid}. The drift velocity in this region is $v_d \approx z_{mid}/t_3 \approx 3.3 \cdot 10^6$ cm/s. Mobility of H^+ ions in the gas phase of the breakdown channel in the region of average electrical field strength is equal to $\mu \approx 40$ cm^2/V·s, according to formula (22).

Conclusion

It can be assumed that the mechanisms of primary and secondary current formation are similar during anodic breakdown in solid and liquid dielectric materials.

The primary processes (including conduction current and breakdown channel movement) are satisfactorily described by the mechanism of free electron generation through interatomic cascade Auger transitions of electrons in the valence band of the dielectric. The primary current density is ~10^4 A, and the channel velocity is ~-10^6 cm/s at an average electric field strength of 10^5 V/cm in solid and liquid dielectric samples.

At high values of electrical field strength (>10^6 V/cm) and relatively long breakdown times (for long samples), the channel walls structurally degrade. The widening of the breakdown channel and the increase in current in the experiment can be attributed to secondary breakdown effects. The secondary current is associated with the movement of ions in the gas phase of the channel. The secondary current density in the final phase of breakdown is several times greater than the primary current density. The maximum value of hydrogen ion mobility in the gas phase of the channel is observed in the water sample (110 $cm^2/V \cdot s$) compared to the transformer oil (40 $cm^2/V \cdot s$) and polyethylene (10 $cm^2/V \cdot s$) samples.

References:

1. Torbin N. M. Pre-breakdown currents in large thicknesses of solid dielectrics. Izv. Vuzov. Energetika. 1960. № 10. pp. 26–31 (in Russian). Experimental study of the breakdown and destruction of solid dielectrics under pulsed voltage. Dissertation. Tomsk TPI, 1961. (in Russian).

2. Sakamoto S., Yamada H. Optical Study of Conduction and Breakdown in Dielectric Liquids. IEEE Trans. on Electr. Insul. 1980. **EI-15**(3), 171.

3. Yamashita H., Amano H. Pre-Breakdown Current and Light Emission in Transformer Oil. IEEE Trans. on Electr. Insul. 1985. **EI-20**(2), 247.

4. Ovchinnikov I.T., Yanshin E.V. Izmereniye predproboynoy elektroprovodnosti vody s pomoshch'yu impul'snogo vysokovol'tnogo elektrooptycheskogo mosta. V kn. Impul'snyy razryad v dielektrikakh. (Izda-vo Nauka, Novosibirsk, 1985), s. 83-88. (in Russian)

5. Yamada H., Kimura S., Sato T. Electro-optical measurement of prebreakdown current and breakdown time lag in polyethylene using nano-second rectangular pulse voltage. *Proceedings of the 3rd International Conference on Conduction and Breakdown in Solid Dielectrics*, Trondheim, Norway, 3–6 July 1989. P. 87–91. DOI: https://doi.org/10.1109/icsd.1989.69167.

6. Vorobyov A.A., Vorobyov G.A. Electricheskiy proboi i razrushenie tverdykh tel (Izda-vo Vysshaya shkola, M., 1966), 224 s. (in Russian)

7. Vershinin, Yu. N. *Elektronno-teplovyye i detonatsionnyye protsessy pri elektricheskom proboye tvyordykh dielektrikov* (Electron-Thermal and Detonation Processes in the Electrical Breakdown of Solid Dielectrics), Yekaterinburg: Ural. Otd. Ross. Akad. Nauk, 2000.

8. Mohan Rao U., Fofana I., Beroual A., Rozga P., Pompili M., Calcara L., Rapp K.J. A Review on Prebreakdown phenomena in Ester Fluids. IEEE Tr. Dielectr. Electr. Insul. 2020. V. 27. № 5. pp. 1546-1560. DOI:10.1109/TDEI.2020.008765

9. Punanov I.F. *Prostranstvenno-vremennye i energeticheskie kharakteristiki vysokovoltnogo nanosekundnogo proboya kondensirovannykh dielektrikov* (Dissertation..Yekaterinburg, UrFU, 2017) (in Russian).

10. Emlin R.V., Morozov P.A., Shcherbakov E. N. A mass-charge measurment of main plasma components generated by the dielectric flashover Technical Physics, 2024, Vol. 69, No. 4. pp. 557-563. https://doi.org/10.61011/JTF.2024.04.57529.194-23

11. Emlin R.V., Morozov P.A., Punanov I.F., Lisenkov V.V. Shcherbakov Ye.N. High-Power Plasma Flows Generated by Nanosecond Vacuum Surface Flashover of Polymeric Materials at 80 kV. IEEE Trans. Plasma Sci. 2019. V.47. №. 6. P. 2838, doi: 10.1109/TPS.2019.2914335

12. Kulikov V. D. The mechanism of the streamer stage of breakdown in crystal dielectrics. Tech. Phys. Lett. 2000. V. 26. № 2. pp. 170-172. DOI: 10.1134/1.1262781

13. Kulikov V. D. Charge Carrier Generation in a KBr Crystal under the Action of a Pulsed Sub-Breakdown Electric Field. Tech. Phys. Lett. 2002. V. 28. № 2. pp. 99-101.

DOI: 10.1134/1.1458502

14. Kulikov V. D. Electrical Breakdown in Ionic Crystals Exposed to Nanosecond Pulses. Tech. Phys. 2003. V. 48. № 12. pp. 1527-1531. DOI: 10.1134/1.1634672

15. Kulikov V. D. Electrical Breakdown in Ionic Crystals. Tech. Phys. 2009. V. 54. № 1. pp. 56-61. DOI:10.1134/S1063784209010083

16. Kulikov V. D. Model of the Electrical Breakdown Channel in Ionic Crystals. Tech. Phys. 2012. V. 57. № 2. pp. 192-197. DOI:10.1134/S1063784212020144

17. Emlin R. V., Barakhvostov S. V., Kulikov V. D. Anisotropy of Electrical Breakdown in Crystalline Quartz. Tech. Phys. 2009. V. 54. № 7. pp. 1076-1079. DOI:10.1134/S1063784209070275

18. Punanov I.F., Emlin R. V., Kulikov V. D. and Cholakh S.O. Resistance of a Pulsed Electrical Breakdown Channel in Ionic Crystals. Tech. Phys. 2014. V. 59. № 4. pp. 503-507. DOI: 10.1134/S1063784214040197

19. Kulikov V., Yakovlev V., Bobkova L. Model of a streamer discharge channel in monocrystalline CdS. Norw. J. Dev. Int. Sci. 2020. № 44-1. pp. 21-24.

20. Kulikov V. Electrical breakdown of polymeric materials. Norw. J. Dev. Int. Sci. 2021. № 62-1. pp. 51-54. DOI:10.24412/3453-9875-2021-62-1-51-54

21. Kulikov V. Barrier effect in dielectric materials. Norw. J. Dev. Int. Sci. 2023. № 103. pp. 47-52. doi. org/10.5281/zenodo.7688048

22. Kulikov V.D. A review on anodic electrical breakdown phenomena in dielectric materials. Norw. J. Dev. Int. Sci. 2024. №. 128, P. 31. doi: 10.5281/zenodo.10817074

23. Emlin R.V., Punanov I.F., Kulikov V.D. Electronic mechanism of propagation of nanosecond breakdown channel in liquid organic dielectrics. Tech. Phys. 2022. V. 92. № 10. pp. 1342-1348. DOI: 10.21883/TP.2022.10.54361.93-22

24. Kulikov V. Electric Breakdown in Water. *Norw. J. Dev. Int. Sci.* 2023. № 118. pp. 50-54.
doi. org/10.5281/zenodo.10009518

25. Kulikov, V.D. Pre-breakdown phenomena in dielectric materials. Norw. J. Dev. Int. Sci. 2024, № 146. p. 126. https://doi.org/10.5281/zenodo.14499282

26. Emlin R.V., Punanov I.F., Kulikov V.D. Fast Breakdown Phenomena in Condensed Dielectrics under Pulsed Voltage Conditions. *Bulletin of the Russian Academy of Sciences: Physics. 2025, Vol. 89, No. 10, pp. 1880–1888.* **DOI:** 10.1134/S1062873825712693

27. Bonch-Bruevich, V.L. and Kalashnikov S.G., *Fizika poluprovodnikov* (Physics of Semiconductors), Moscow: Nauka, 1977.

28. Spice J.E. Chemical Binding and Structure. New York: Pergamon Press, 1964

29. Nemoshkalenko V. V and Aleshin V. G. Electron Spectroscopy of Crystals (Naukova Dumka, Kiev, 1976; Plenum, New York, 1979).

30. Meek J.M., Craggs J.D. Electrical Breakdown of Gases. (Oxford: Clarendon Press, 1953). 507

31 Behrisch R. Sputtering by Particle Bombardment. (Springger- Verlag, Berlin- Heidelberg- N.Y.-Tokio, 1983)

32. Manukhin V.V. Sputtering of carbide films from the surface of the metal by helium ions bombardment. Technical Physics, 2022, Vol. 67, No. 11. P. 1500

33. Zhao L., Su J. C. and Liu C. L. Review of developments on polymers' breakdown characteristics and mechanisms on a nanosecond time scale. AIP Advances 2020. V.10. 035206. https://doi.org/10.1063/1.5110273

34. Ushakov V. Ya. Impul'snyy elektricheskiy proboy zhidkostey. (Izda-vo Tomsk St. Univ. Tomsk, 1975). 258 s. (in Russian).

35. Bin C., Ji-Wei D., Ming-He C. Electrical Breakdown Mechanism of Transformer Oil with Water Impurity: Molecular Dynamics Simulations and First-Principles Calculations. Crystals. 2021. V. *11*. № 2. P. 123. DOI: 10.3390/cryst11020123